Title

Structural Behaviour of Composite Timber Beams with Densified Wooden Nail Connections: Modelling Strategies and Experimental Validation

Abstract

This study investigates laminated composite beams assembled with densified wooden nails through experimental testing, finite element modelling, and analytical methods. Single shear tests characterise connection stiffness and reveal a limited elastic range. A Foschi constitutive law is adopted to capture the non-linear load-slip behaviour and incorporated into beam-scale models.

Four modelling strategies are compared at beam scale: finite element and Girhammar analytical approaches, each with linear-elastic or non-linear connection assumptions. The predictive accuracy is assessed through deflection predictions. The non-linear finite element model demonstrates the highest accuracy. Under linear-elastic assumptions, the Girhammar method provides exact agreement with finite element results. When extended to non-linear behaviour, the analytical model overestimates deflections due to simplifying assumptions concerning the connection stiffness along the span. Full-scale three-point bending tests are used to validate these modelling approaches. For the specific beam configuration and the limited experimental dataset tested, the results indicate that the elastic limit is reached before conventional serviceability thresholds (L/250). This observation underscores the importance of incorporating connection non-linearity to accurately predict the structural behaviour of beams assembled with densified wooden nails.

Keywords

- → Nailed Laminated Timber Beams
- → Densified wooden nails
- → Semi-rigid connections
- → Finite element modelling
- → Girhammar analytical method
- → Non-linear modelling

Article

1. INTRODUCTION

Context

The construction industry is a primary contributor to global CO_2 emissions, necessitating a shift towards sustainable practices [1]. Timber construction has received growing interest [2], [3] due to its potential role in climate change mitigation, notably through carbon sequestration [4], [5]. In addition, wood is a renewable, lightweight material with favourable mechanical properties [4], which has led to the development of Engineered Wood Products (EWPs) [6], [7].

However, EWPs typically rely on synthetic adhesives and metallic fasteners, which limit recyclability and material separation at end-of-life [8], [9], reducing resource circularity in timber systems [10], [11], [12], [13]. To address this, metal-free and adhesive-free connection systems have been increasingly explored. Densified wood technology, which uses thermo-mechanical treatment to enhance material properties [14], [15], [16] has enabled the development of wood-based fasteners for *Dowel-Laminated Timber (DLT)* and similar systems [17].

To date, densified wood connectors have been predominantly investigated as structural dowels. Reviews of these systems have highlighted that standard design frameworks, such as Eurocode 5 [18], often fail to accurately predict their performance, as they neglect the deformability and specific shear failure modes of the wooden fastener [19]. Furthermore, at the structural scale, multi-layered panels assembled with wooden dowels (such as DLT) typically provide sufficient load-bearing capacity but exhibit relatively low bending stiffness, typically achieving only 10% to 20% of their glued equivalents [16].

While the structural behaviour of large-diameter dowels is increasingly documented, the use of densified wooden nails as structural fasteners remains largely unexplored [19]. Nevertheless, densified wooden nails are already employed in various non-structural applications, including fencing, furniture [20], and pallet assemblies [21], as well as in solid timber construction [22], [23], [24], [25], [26]. Previous studies have demonstrated their structural potential, particularly in the context of salvaged timber reuse [27], [28] and restoration works [29], [30]. Wooden nails offer several advantages, including rapid assembly, suitability for prefabrication [31], and installation without pre-drilling in softwood [16]. However, the available literature on their structural mechanical behaviour remains limited [16], [19], [32], [33], [34], [35], thereby limiting their integration into engineered timber systems and standard design frameworks.

Objectives and scope of the study

This study addresses the current lack of experimental data and predictive modelling frameworks for structural wooden nails in laminated composite beams. The conclusions drawn in this work are limited to the investigated beam configuration and loading conditions.

To achieve this, the research adopts a multi-scale methodology. At the connection scale, wooden nail connectors are characterised through combined analytical and experimental investigations. The non-linear load-slip behaviour is modelled using the Foschi law, which provides the constitutive relationship required for beam-scale simulations. At the beam scale, numerical and analytical modelling approaches are developed and compared. A finite element model (FEM) is implemented to provide a robust framework for incorporating non-linear connection behaviour. In parallel, a brief review of existing analytical methods confirms the selection of the Girhammar Generalised Exact Method as a computationally efficient alternative.

Four modelling strategies are compared, combining numerical and analytical approaches with either linear-elastic or non-linear connection assumptions. The study focuses on predicting beam deflections at serviceability load levels. The predictive accuracy of the proposed modelling strategies is validated through comparison with experimental data from full-scale three-point bending tests.

2. SINGLE SHEAR CONNECTIONS USING A DENSIFIED WOODEN NAIL

2.1 Overview

This section presents the mechanical characterisation of a single-fastener shear joint, which yieldsthe input parameters required to model composite beams assembled with densified wooden nails. Both experimental and analytical approaches are used to characterise the connection. The experimental shear strength of the connection is compared with calculated values derived from Eurocode 5 (EC5) [18] and European Technical Assessment (ETA) [36] design recommendations. In parallel, slip moduli are determined experimentally according to the ISO 6891:1983 procedure [37] and compared with analytically predicted values. Finally, the Foschi approach [38] is used to model the non-linear load-slip behaviour of the joint.

2.2 Experimental Characterisation: Single-Shear Tests

2.2.1 Materials

The connectors investigated in this study are ***LIGNOLOC®*** densified wooden nails (***BECK***, Austria) [39], [40], which are manufactured from resin-impregnated beech wood subjected to unidirectional densification. The nails are high-speed driven into timber using a pneumatic gun. The frictional heat causes lignin to weld between the nail and surrounding fibres, resulting in a higher withdrawal resistance than the one typically obtained with manually driven fasteners [41], [42]. However, the lignin-based bond remains moisture-sensitive [20], [41], [43], [44]. The geometric and mechanical specifications are summarised in Table 1.

Nominal length [mm]	65/90
Nominal diameter [mm]	5.3
Characteristic yield moment [Nmm]	3600
Characteristic tensile capacity [kN]	2.0
Withdrawal strength [N/mm²]	7.0

Table 1 - Properties of LIGNOLOC® wooden nails [36]

The timber members are made from European silver fir (Abies alba). The wood density was measured at 478 ± 32 kg/m³ with an initial moisture content (MC) of 9.3 ± 0.3%, according to standards [45], [46].

2.2.2 Connection Specimens

Single shear specimens are composed of two timber members (30 x 120 x 250 mm) connected by a single headless wooden nail (diameter d = 5.3 mm). To ensure maximum penetration depth into both boards, 90 mm long wooden nails were used, resulting in the nail protruding from both sides of the assembly. The F60 CN15-PS90 pneumatic gun was used. Geometrical specifications of the connection specimens are shown in Figure 1.

A total of 33 specimens were tested.

2.2.3 Testing Procedure for Single-Fastener Joint

To avoid parasitic bending moments induced by standard arch-type test setups and to characterise a single shear plane, a loading setup proposed by Pirazzi [47] was adopted. This setup involves tilting the two-part assembly to apply compressive loads at both ends. The fastener is thereby subjected to an almost pure shear loading condition [48]. The loading procedure followed the force control protocol described in ISO 6891:1983 [37], implemented via a 300 kN capacity universal testing machine.

Displacement was recorded by two linear variable differential transformers (LVDTs) positioned on each side of the shear plane, with the final value calculated as the mean of both measurements.

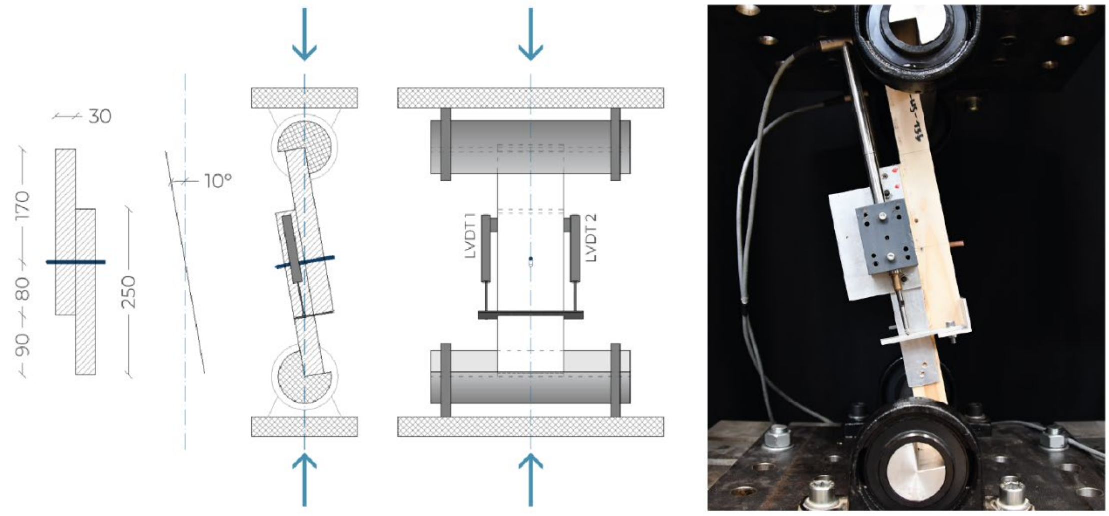

Figure 1 - Single shear test specimen and testing set-up

2.2.4 Experimental results

Data and results of all specimens are presented in Appendix 6.1.1, Table 9.

The failure mechanism observed in the tested specimens involved the formation of double plastic hinges in the fasteners (Figure 2). This failure mode corresponds to ***mode f*** as defined in EC5 for timber-based connections [18], consistent with findings by Wang et al. for similar joint configurations [33]. These hinges are less pronounced than those typically observed in conventional steel fasteners. The average shear strength is 1258.33 ± 162.56 N.

The resulting load-slip curves $(P - \Delta)$ are presented in Figure 2. They reveal considerable variability in the connector's response. Linear slip moduli K_{ser} were derived from the mean load-slip curve and its variation limits (Table 2), according to ISO 6891:1983 [37] (Appendix 6.1.2, Eq. (5) & (6)).

The experimental curves exhibit non-linear behaviour with a very short or negligible linear elastic phase. The non-linear behaviour was described by an explicit mathematical formulation using the Foschi law, expressed in Eq. (1) - [38], [49]. The curves were calibrated using the post-unloading part of the mean load-slip responses. This choice enables the isolation of the intrinsic mechanical behaviour of the connection by excluding the effects of initial slip. Foschi parameters were determined via non-linear least squares (Table 2). The fitting quality was assessed using the coefficient of determination (R^2), Mean Absolute Error (MAE), and Root Mean Squared Error (RMSE).

$$P = (F_0 + K_1\delta) \cdot [1 - e^{\left(\frac{-K_0\delta}{F_0}\right)}] \tag{1}$$

where:
P: load;
δ: slip;
K_0: elastic stiffness of the connection;
K_1: plastic stiffness of the connection;
F_0: intercept of the plastic stiffness tangent.

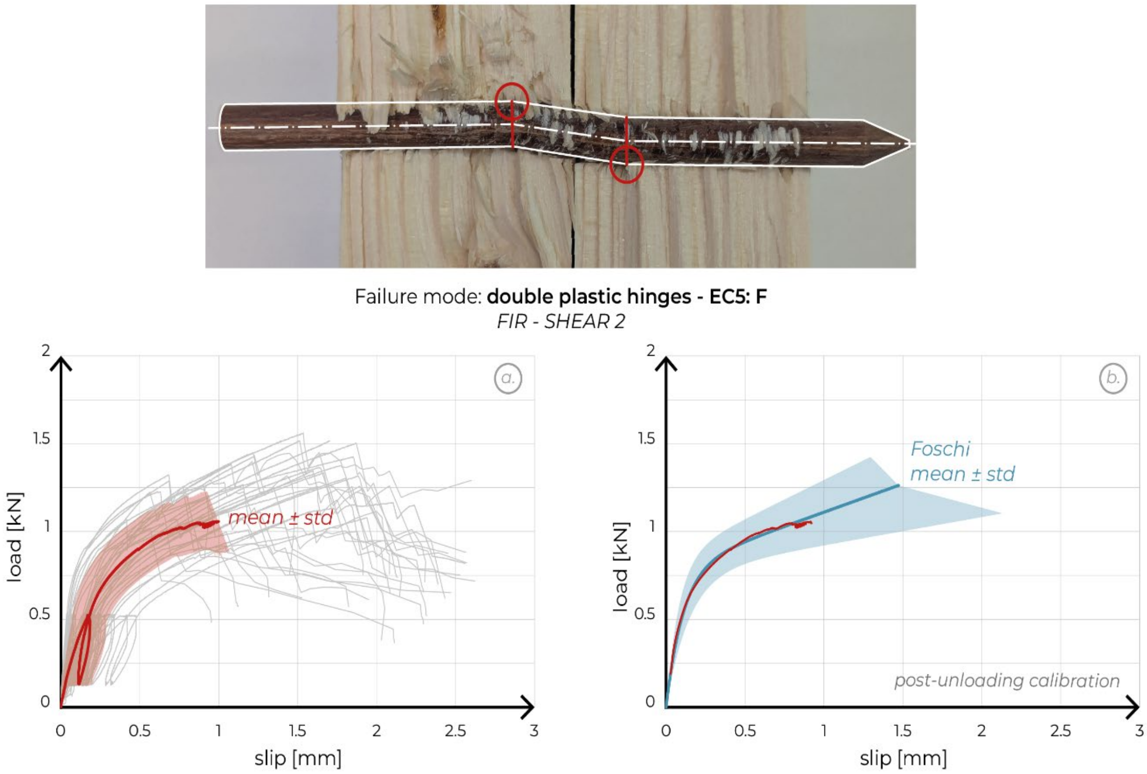

Figure 2 - Typical failure mode in shear tests and mechanical behaviour.
a) Load-slip curves and average behaviours (mean ± std.). b) Foschi's curves on post unloading calibration.

		Experimental		Foschi curve approximation					
		F_{vrd} [N]	K_{ser} [N/mm]	K_0 [N/mm]	K_1 [N/mm]	F_0 [N]	R^2 [-]	MAE [N]	RMSE [N]
n = 33	mean	1258.33	2760.54	7617.60	323.00	787.36	0.993	14.40	16.49
	mean + std	1420.90	5639.65	10773.65	444.81	848.76	0.991	15.90	19.24
	mean - std	1095.77	1827.55	5312.12	160.87	761.27	0.994	12.72	14.37

Table 2 - Single shear tests: experimental shear strength and stiffness results (average and variation limits) | Foschi parameters and fitting quality.

2.3 Analytical Estimation of Connection Properties Based on Standards

This section provides analytical estimations of the connection properties based on standard formulations, which are subsequently compared with the experimentally measured values.

2.3.1 Eurocode 5

EC5 [18] provides analytical formulations to estimate the mechanical properties of mechanically fastened timber joints. Clause 11.2.3 applies Johansen's yield theory to predict lateral resistance of a fastener loaded in a single shear plane ($F_{v,Rk}$) and the associated failure modes (Appendix 6.1.3, Eq. (7)). In addition, clause 11.3.8 provides an empirical formulation for slip modulus of smooth nails driven without pre-drilling (Appendix 6.1.3, Eq.(8)).

Furthermore, as specified in EC5 (Clause 11.2.3.4) [18], the coefficients of 1.15 and 1.05—originally introduced for steel fasteners [50]—should be replaced by 1.0 when applied to wooden connectors. Given the very limited deformations observed during testing, the contribution of the rope effect $\left(F_{ax,Rk}/4\right)$ was neglected.

For comparison with experimental results, all characteristic analytical values were replaced by mean values measured on specimens. The fastener yield moment is taken from ETA [36]. The calculated values are reported in Table 3.

2.3.2 European Technical Assessment (ETA)

The European Technical Assessment [36] provides an alternative analytical framework to estimate the mechanical properties of the connection. The ETA reports characteristic resistance and stiffness values together with the corresponding analytical formulations (Eq. (9) and Eq. (10)). All characteristic analytical values were replaced by mean values measured on specimens, except for the fastener yield moment, which is taken directly from the ETA [36]. The calculated values are reported in Table 3.

	Experimental		EC5		ETA	
	ρ [kg/m³]	F_{v_EXP} [N]	F_{v_EC5} [N]	K_{ser_EC5} [N/mm]	$F_{v,ETA}$ [N]	K_{ser_ETA} [N/mm]
Mean	477.98	1258.33	951.44	1727.31	823.97	2746.58
STD	31.78	162.57	27.88	153.96	24.14	80.47
COV	6.7%	12.9%	2.9%	8.9%	2.9%	2.9%

Table 3 - Experimental and analytical strength and stiffness properties for single shear joint with a wooden nail.

2.4 Comparisons and Discussion

Analytical models provide conservative estimates of the load-carrying capacity when compared to experimental results (F_{v_EXP}= 1258.33 N). The EC5 formulation (F_{v_EC5}= 951.44 N) underestimates the experimentally measured maximum load by approximately 25%, while the ETA-based prediction (F_{v_ETA}= 823.97 N) shows a larger deviation of approximately 35%. Despite this underestimation, the EC5 predictions are consistent with the experimentally observed ***failure mode f***.

When the rope effect is included—following the approach of Wang et al. [33]—the EC5 formulation provides a closer agreement with the experimental results ($F_{v\_EC5} + \frac{F_{ax}}{4}$= 1133.55 N). However, this improved agreement should be interpreted with caution, as the very small connector deformations observed in the tests do not provide strong physical evidence of a significant rope contribution in the present configuration [51]. In this context, the main sources of discrepancy between predicted and measured values are more plausibly associated with modelling assumptions and material parameters, such as variations in local embedment strength, uncertainties in the assumed yield moment of the densified fastener, and the use of mean values within characteristic-based formulations, rather than the activation of a pronounced rope effect.

Regarding joint stiffness, the experimentally derived slip modulus (K_{ser_EXP}= 2760.54 N/mm) is highly consistent with the ETA-based calculation (K_{ser_ETA}= 2746.58 N/mm). In contrast, the EC5 formulation underestimates the connection stiffness for this type of fastener (K_{ser_EC5}= 1727.31 N/mm). For comparison within the beam modelling framework, the stiffness of a 12 mm diameter wooden dowel, calculated according to EC5 by Eq. (8), is also reported (K_{dowel}= 5174.66 N/mm).

These stiffness values all account for the initial slip of the connection and assume linear-elastic behaviour. However, as shown by the experimental load-slip curves, the connector response is predominantly non-linear. To account for this behaviour in subsequent beam modelling, the post-unloading response of the connection was approximated using a Foschi formulation (Table 2).

3. COMPOSITE BEAMS WITH DENSIFIED WOODEN NAILS

3.1 Overview

This section evaluates the predictive accuracy of numerical and analytical models for composite beams assembled with densified wooden nails (*Nailed Laminated Timber – NLT*). The mechanical parameters identified at the connector scale (Section 2)—specifically the slip modulus and non-linear load-slip behaviour—are used as input parameters for the beam-scale models.

A composite beam subjected to three-point bending serves as the reference configuration for evaluating different modelling strategies. The beam is composed of five lamellae with geometric and nailing specifications detailed in Section 3.4. This configuration was selected to apply a relatively uniform load to the fasteners along the beam (Appendix 6.2.3).

The investigation is structured as follows:

- *Numerical Simulation:* A finite element model (FEM) is established to capture the non-linear behaviour of the connection.
- *Analytical Framework:* Existing analytical approaches for timber beams with semi-rigid connections are briefly reviewed. The Girhammar Generalised Exact Method is adopted as a computationally efficient analytical solution.
- *Experimental Validation:* The predictive accuracy of both modelling approaches is assessed through comparison with full-scale experimental tests.

3.2 Numerical Model

A finite element model (FEM) is developed as a primary modelling tool in this study. It provides an efficient implementation of the non-linear behaviour of densified wooden nail connectors identified at the unit scale.

Numerical simulations were performed using the finite element software ***SCIA Engineer*** (Nemetschek Group) [52], an engineer-oriented solution used by practitioners.

3.2.1 Elements and Interface

The modelling strategy adopts a two-dimensional approach where each lamella is explicitly represented using plane stress elements (2D membrane). This modelling approach assumes a uniform stress distribution across the beam width.

The mechanical interaction at the interfaces is governed by a continuous spring model. As illustrated in Figure 3, the interaction between adjacent lamellae is defined by three stiffness components:

- *Transverse stiffness ($\mathrm{k_Z} \rightarrow \infty$):* This is assumed to be fully rigid to ensure displacement compatibility and prevent interpenetration between layers.
- *Rotational stiffness ($\mathrm{k_\theta} = 0$):* This is defined as free to allow independent bending of the lamellae, consistent with non-glued assemblies.
- *Longitudinal stiffness ($\mathrm{k_X}$):* This represents the shear connection provided by the fasteners. In this study, k_X is derived from the slip moduli (K) obtained from experimental characterisation and analytical standards.

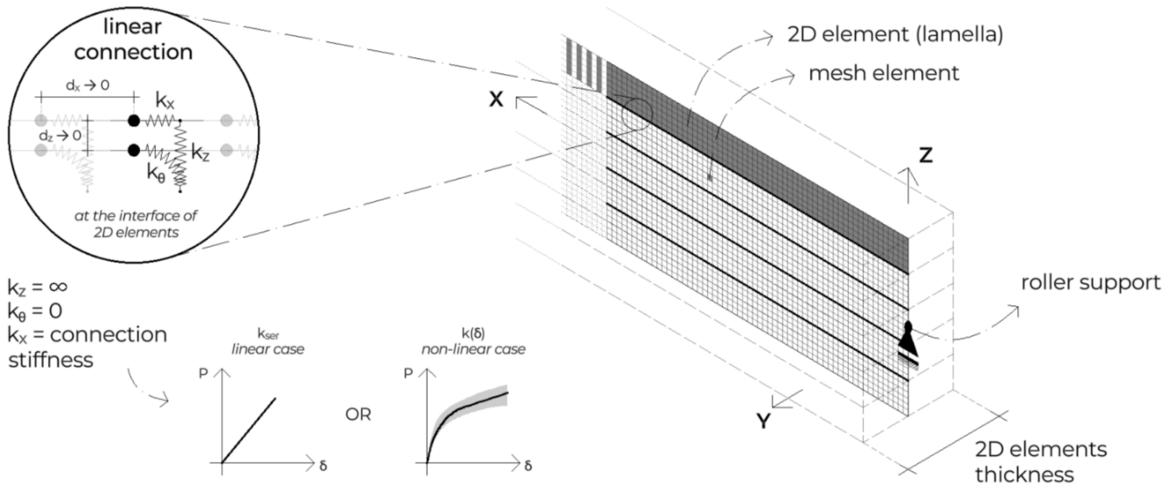

Figure 3 - Finite Element Modelling for interface connection of 2D elements (lamellae) – Roller support zone.

3.2.2 Material

Timber lamellae are modelled as linear elastic materials. The modulus of elasticity is assigned to each lamella individually and assumed constant along the beam length. To maintain consistency with the analytical formulation (Section 3.3), shear deformation within the lamellae is neglected by assigning a sufficiently large shear modulus ($G \to \infty$). This assumption is justified by the dominance of connector-induced shear deformations. Its influence was verified numerically using a finite shear modulus (G = 690 N/mm², [53]), leading to less than a 3% difference in mid-span deflection.

3.2.3 Boundary and Loading conditions

Symmetrical roller supports at both ends of the central lamella allow longitudinal displacement while preventing vertical translation. A fictitious support at midspan restrains translation in the x-direction to prevent rigid-body motion. This constraint ensures numerical stability without affecting the internal force distribution or global response.

To limit the influence of local stress concentrations near the loading point, the external load is distributed over the entire height of the beam.

3.2.4 Mesh

Each lamella is meshed using four-node quadrilateral plane stress elements with a mesh size of 5 x 5 mm, resulting in 3120 elements per lamella. These elements use four integration points, from which results are extrapolated and averaged at the nodes. This discretisation was selected following a sensitivity study (Appendix 6.2.1), which confirmed that further mesh refinement did not lead to more accurate results.

3.2.5 Non Linearities

The non-linear model incorporates the connection behaviour through the longitudinal stiffness (k_X) defined by the experimentally calibrated Foschi law (Figure 3).

To isolate the specific influence of connection non-linearity, neither geometric nor material non-linearities were considered.

3.3 Analytical Model

While the numerical model provides deep insights into structural behaviour, the considered modelling complexity limits its practical use for iterative design and optimisation studies. To complement this approach, analytical formulations have been investigated to describe mechanically assembled composite timber beams with semi-rigid shear connections.

3.3.1 Analytical methods

For timber applications, the most suitable formulations include the Gamma Method, the Shear Analogy Method, and the Girhammar's Generalised Excat Method.

The ***Gamma Method***, as described by Heimeshoff [54] and presented in EC5-Annex B5 [55], uses a reduction coefficient (γ) to account for partial composite action. A value of $\gamma = 1$ represents a fully composite beam, while $\gamma = 0$ represents a system without connectors. Although widely used in design practice, the standard formulation is limited to three-layered elements and is derived under the assumption of a sinusoidal load distribution [56]. Extensions to multi-layered assemblies have been proposed, but they remain based on the same underlying loading assumption [57].

The ***Shear Analogy Method***, proposed by Kreuzinger [58], transforms a mechanically jointed composite beam into a fictitious homogenised system composed of two coupled components, denoted A and B. Component A represents the sum of the bending stiffnesses of the individual layers, expressed as $(EI)_A = \sum_{i=1}^{n}(EI)_i$. Component B accounts for the composite action through the Steiner component of the bending stiffness $(EI)_B$, as well as a shear stiffness (S_B) including individual shear deformation of components and joint slip induced by the semi-rigid connection. Unlike the γ-method, this approach is applicable to arbitrary load configurations and multi-layered systems [56].

The ***Generalised Exact Method*** of Girhammar is based on the exact solution of the equilibrium equations governing axial (u_i) and transverse (w) displacements of the layered system [59], [60]. Initially developed for two-layer beams, a generalisation for multi-layered beams was proposed by L. Resch [48]. This approach is valid for arbitrary loading conditions.

A synthetic comparison of these analytical approaches is provided in Table 4. The *Girhammar Generalised Exact Method* was selected for this study as it directly solves the exact equilibrium equation while preserving clear physical interpretation of interlayer slip, without using homogenisation or equivalent stiffness representations. Unlike the *Shear Analogy Method,* it neglects individual lamella shear deformation.

method	multi-layer capability	loading assumptions	individual shear deformation	composite action	resolution approach
Gamma Method (EC5)	Limited (3-layer systems; extensions available)	Sinusoidal (assumed)	No	Reduction coefficient (γ)	Simplified form
Shear Analogy Method (Kreuzinger)	Yes	General	Yes	Equivalent shear stiffness (S_B)	Homogenised beam analogy
Generalised Exact Method (Girhammar)	Yes	General	No	Explicit connector stiffness	Exact equilibrium equations

Table 4 - Comparative overview of analytical methods for composite timber beam modelling

3.3.2 Model inputs and Mechanical Assumptions

Material and geometric properties

The model incorporates the individual mechanical properties for each of the lamellae. This includes the modulus of elasticity (MOE) and the geometric cross-section (b_i x h_i). While the MOE can vary from one layer to another, it is assumed constant along the entire span of a single lamella. For this study, these values were assessed experimentally to ensure a direct comparison (Section 3.4).

Connection behaviour

The mechanical interaction between adjacent lamellae is modelled by an equivalent shear connection characterised by its stiffness–slip relationship. Two modelling strategies are considered:

- *Linear case:* A constant slip modulus is assigned to the interface. This value can be derived from experimental characterisation or determined via design standards.
- *Non-linear case:* To capture the progressive reduction in connection stiffness, an iterative secant stiffness approach—analogous to the Newton-Raphson process—is implemented. The stiffness is derived from a non-linear constitutive law. In this procedure, the connection stiffness is updated iteratively based on the maximum predicted local slip at the interface until the global displacement response converges. A detailed description of the non-linear analytical procedure is provided in Appendix 6.2.2.

In the analytical framework, the connection stiffness is assumed to be homogeneous along the beam span. In the non-linear case, this assumption neglects the spatial variation of slip and stiffness, as connectors subjected to lower slip levels would retain higher stiffness than those located in regions of maximum slip. This simplification generally leads to conservative predictions of global stiffness and deformation. The implications of this assumption for a three-point bending configuration, compared to other loading scenarios, are briefly discussed in Appendix 6.2.3.

3.4 Experimental: Three-point Bending Tests

3.4.1 Materials

Consistent with the single shear tests presented in Section 2, the timber species used for the beam specimens is silver fir (Abies alba). The mechanical properties of each individual lamella were characterised prior to assembly. MOE was determined through four-point bending tests using a localised measurement protocol (Appendix 6.2.4, Figure 8). Multiple measurements were taken to account for the spatial variability of the material properties along each lamella.

The physical and mechanical properties are summarised in Table 5.

The fasteners used were 65 mm long, headless densified wooden nails. Their properties are described in Section 2.2.1.

3.4.2 Beam Specimens

A total of three composite beams (*BEAM 0, 1, and 2*) were fabricated and tested. Each beam consists of five lamellae (*LAM 1 → 5*) with nominal dimensions of 3000 x 120 x 30 mm. Figure 4 presents the geometric configuration and nailing layout of the tested beams.

Adjacent lamellae were connected using wooden nails arranged in a staggered pattern. The spacing between connectors was set to 65 mm, corresponding to the minimum spacing specified in EC5 (Table 11.16) [18].

3.4.3 Testing Procedure for Beams

The experimental tests were carried out according to EN 408 [61], using a three-point bending configuration on beams with a span L of 2600 mm. The load was applied at midspan. To isolate the mechanical response associated with interlayer slip and to enable direct comparison with the analytical modelling of the connection behaviour, a load–unload–reload protocol was applied, with an initial loading stage up to 2000 N. The analysis focuses on the post-unloading phase.

Two LVDTs were positioned beneath the load, one on each side of the beam's cross-section. This arrangement allows the measurements to be averaged and reduces the influence of any local rotation of the cross-section.

	BEAM 0		BEAM 1		BEAM 2	
	ρ [kg/m³]	MOE [N/mm²] *(n=3*)*	ρ [kg/m³]	MOE [N/mm²] *(n=9*)*	ρ [kg/m³]	MOE [N/mm²] *(n=9*)*
LAM 5	476	11680 (±689)	520	15596 (±1839)	547	15159 (±2397)
LAM 4	468	8383 (±1147)	475	12211 (±1059)	406	12716 (±752)
LAM 3	438	7634 (±181)	447	13102 (±1385)	420	9884 (±1332)
LAM 2	404	8899 (±743)	463	10260 (±1150)	514	13028 (±1635)
LAM 1	476	10177 (±711)	463	13382 (±913)	517	14425 (±1260)

*Table 5 - Beam lamellae properties – Moisture content (MC) determined according to EN 13183-1:2002 [46], MC = 10.4 % (±0.4 %). * n = number of MOE measurements per lamella.*

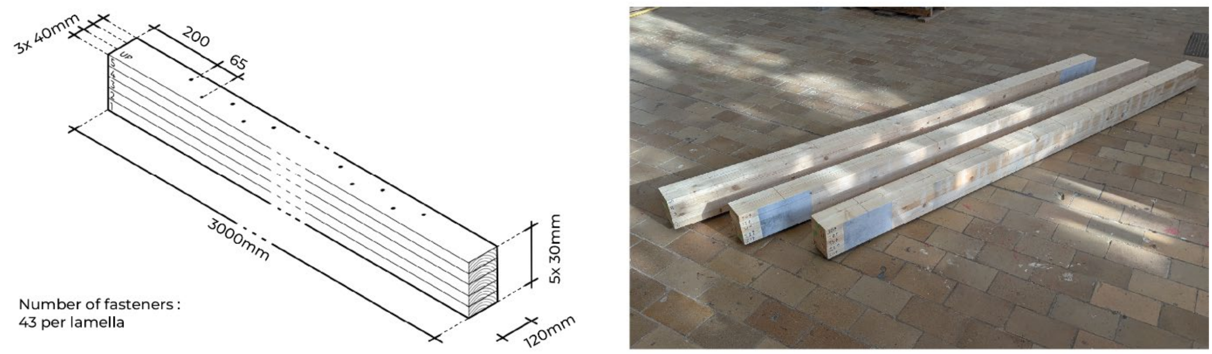

Figure 4 - Geometry of tested beams.

4. RESULTS AND DISCUSSION

4.1 Experimental Structural Response

To enable a consistent comparison between experimental results and model predictions, specific load levels were highlighted to characterise the structural response at commonly defined Serviceability (*SLS*) and Ultimate (*ULS*) limit states:

- *SLS Standard ($F_{w=L/250}$):* corresponds to the standard deflection limit (10.4 mm for the considered geometry).
- *SLS Severe ($F_{w=L/100}$):* a higher threshold (26.0 mm) used to observe the evolution of the beam's behaviour under significant deformation.
- *ULS Load (F_{ULS}):* defined as $1.5 \times F_{w=L/100}$. Beyond this value, the design criterion is governed by SLS deformation limits rather than load-carrying capacity.
- *Ultimate Failure Load (F_{max}):* the maximum load recorded experimentally before total structural failure.

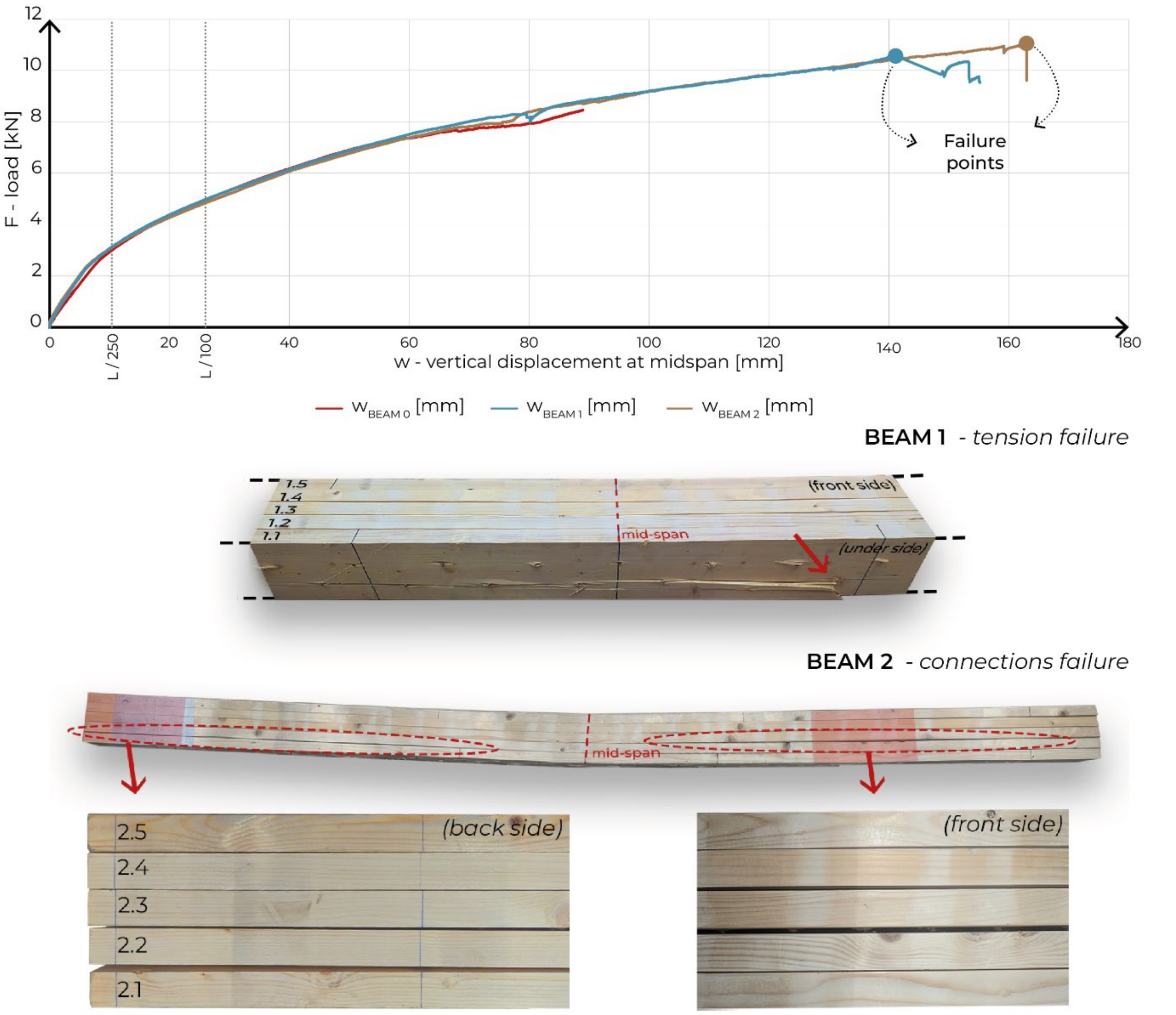

Figure 5 - Load-slip curves for all beam specimens tested (BEAM 0, BEAM 1 and BEAM 2) and corresponding failure modes. BEAM 0 was not loaded to complete failure.

The global response of the tested beams (*BEAM 0, 1, and 2*) is illustrated in Figure 5. Despite the limited number of specimens, the curves demonstrate a high degree of consistency, with only minor variation in stiffness, suggesting a reproducible structural response for the investigated configuration.

As observed at the connector scale (Section 2.2), the composite beams exhibit non-linear behaviour at early loading stages. Even at the standard serviceability limit ($\mathrm{L}/250$), the structural response suggests that the elastic limit has already been exceeded. While this observation is consistent across all tested beams, it should be interpreted cautiously due to the limited experimental dataset. Nevertheless, it highlights a potentially important aspect regarding the interpretation of serviceability limits when irreversible deformation mechanisms may occur at relatively low load levels.

Table 6 presents the experimental values for each tested beam. For clarity of comparison, *BEAM 1* is used as the reference specimen in the main discussion, as the overall trends and conclusions are consistent across all beams. Since each beam is modelled using its own material properties, the detailed results for *BEAM 0* and *BEAM 2* are available in Appendices 6.2.5 and 6.2.6.

	SLS		ULS		ductility definition				
	$F_{w=L/250}$ [kN]	$F_{w=L/100}$ [kN]	F_{ULS} [kN]	w_{ULS} [mm]	F_{max} [kN]	v_u [mm]	F_y [kN]	v_y [mm]	D_s [-]
BEAM 0	3.00	4.96	7.43	62.75	–[1]	–[1]	3.75	12.88	–[1]
BEAM 1	3.12	4.98	7.46	59.20	10.57	141.15	3.50	9.75	14.46
BEAM 2	3.11	4.84	7.26	57.73	11.19	162.96	3.18	9.26	17.60
mean	3.08	4.92	7.39	59.89	10.88	152.05	3.48	10.63	16.03
std	0.06	0.06	0.09	2.11	0.31	10.90	0.23	1.60	1.57

Table 6 - Characteristic load levels and ductility for tested beams. [1]BEAM 0: *not loaded to failure.*

For specimen *BEAM 0*, the test was stopped before complete failure. The failure mechanisms varied for the two other specimens. Specimen *BEAM 1* failed through tensile rupture of the lower lamella, indicating flexural failure governed by timber strength. In contrast, specimen *BEAM 2* exhibited a failure associated with damage to the connectors, primarily at the interfaces between lamellae 2.1–2.2 and 2.2–2.3 (Figure 5).

The ductility of the composite beams is quantified using the ductility ratio D_s, defined by Eq. (2), with v_u is the displacement at ultimate load and v_y is the displacement at the yield point (defined according to EN 12512 [62]):

$$D_s = \frac{v_u}{v_y} \tag{2}$$

The beams tested up to failure reached a mean ductility ratio of 16.03. Although this value was derived from only two specimens and should therefore be interpreted cautiously, all tested beams consistently exhibited a pronounced non-linear and ductile response. Compared with the brittle behaviour typically reported for glued laminated timber, where ductility ratios are generally lower than 2.0 [63], [64], the investigated system has the potential to provide an enhanced post-yield deformation capacity.

4.2 Comparison Between Models

The predictive capability of the different modelling strategies was evaluated at the two previously defined serviceability levels: the standard limit $L/250$ and the severe service limit $L/100$. Table 7 presents the mid-span deflection results for specimen ***BEAM 1***, comparing experimental data (w_{exp}) with model predictions under different assumptions:

- ***Linear Elastic Models:*** Based on experimental stiffness ($w_{NUM\_K.exp}$, $w_{ANA\_K.exp}$) and design standards ($w_{NUM\_K.EC5}$, $w_{NUM\_K.ETA}$);
- ***Non-Linear Models:*** Incorporating the Foschi constitutive law (w_{NUM_NL}, w_{ANA_NL}).

		load [kN]	w_{exp} [mm]	$w_{NUM\_K.exp}$ [mm]	$w_{ANA\_K.exp}$ [mm]	$w_{NUM\_K.EC5}$ [mm]	$w_{NUM\_K.ETA}$ [mm]	w_{NUM_NL} [mm]	w_{ANA_NL} [mm]
BEAM 1	$F_{L/250}$	3.12	10.40	11.77 (*+13.1%*)	11.76 (*+13.1%*)	15.96 (***+53.5%***)	11.80 (*+13.5%*)	10.09 (*-3.0%*)	10.19 (*-2.0%*)
	$F_{L/100}$	4.98	26.00	18.74 (***-27.9%***)	18.73 (***-27.9%***)	25.42 (*-2.2%*)	18.80 (***-27.7%***)	27.70 (*+6.6%*)	30.51 (*+17.3%*)

Table 7 - BEAM 1: Model deflections at serviceability levels. Relative error (%) vs. experimental reference.

Linear Elastic Connection Models

Under linear elastic assumptions, numerical predictions based on either experimentally obtained stiffness K_{exp} or ETA prescriptions K_{ETA} exhibit similar trends. At the standard serviceability limit ($L/250$), these models both slightly overestimate the mid-span deflection (+13%). This can be attributed to initial slip included in the connection stiffness definition, whereas the experimental behaviour reflects post-unloading response. At $L/100$, they significantly underestimate deflection (-28%) likely because they do not capture progressive stiffness degradation and connector plasticity. These tendencies are consistent across the other beam specimens (Appendix 6.2.8, Table 11), where linear models similarly overestimate deflection at L/250 (+17%; +12%) and underestimate it at L/100 (-23%; -30%).

The K_{EC5} model provides accurate predictions at the $L/100$ limit (-2.2%), where a conservative linear estimation corresponds to a degraded structural state. However, at $L/250$, the EC5 formulation significantly underestimates stiffness (+54% in predicted deflection).

Overall, linear models offer a simple first approximation, but they fail to capture non-linear behaviour before standard serviceability limits.

Non-Linear Connection Models

Non-linear numerical simulations show the highest accuracy with relative errors between 3% and 6.6% (Table 7, Figure 6), confirming the importance of accounting for connection nonlinearity. The model effectively captures local variations in slip and stiffness degradation.

The analytical model with non-linear connection behaviour reproduces the general response trend (Figure 6) but overestimates the deflection at higher loads (+17.3%).

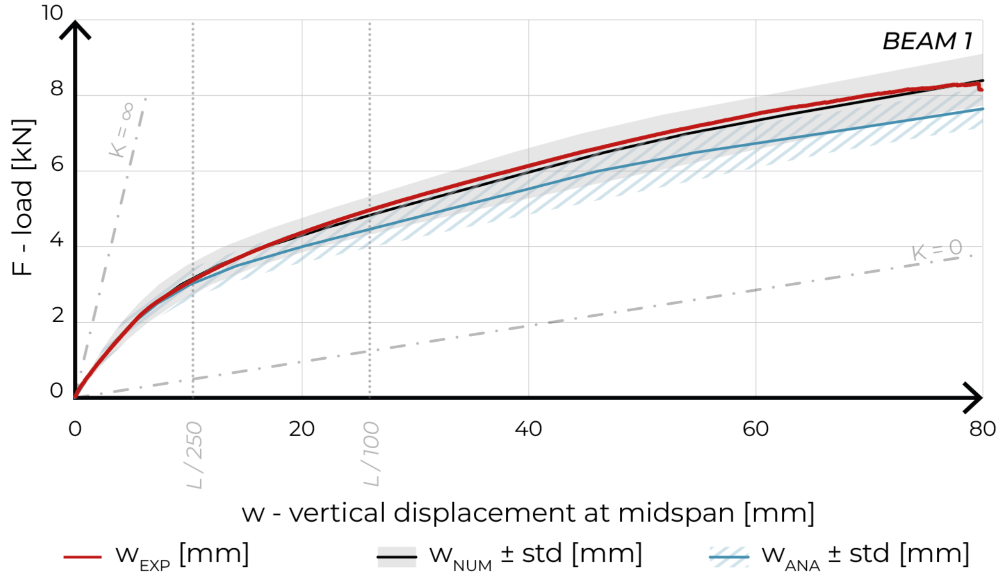

Figure 6 - BEAM 1: Experimental and non-linear models' predictions with variation range. Dashed lines: limit behaviours (K=∞, K=0).

The other beam specimens confirm these observations (Appendix 6.2.8, Table 11), with the non-linear FEM consistently providing the most accurate predictions (−3.0% to +17.1%), while the analytical non-linear model systematically overestimates deformations at higher load levels (+9.9% to +39.7%).

Validation of the Analytical Framework

The exact agreement between numerical ($w_{NUM\_K.exp}$) and analytical results ($w_{ANA\_K.exp}$) under linear assumptions confirms the accuracy of the *Girhammar Generalised Exact Method* (Section 3.3). Under non-linear behaviour, discrepancies arise from the application of a single secant stiffness per interface, which neglects spatial redistribution of slip and forces among fasteners. This artificially softens connectors experiencing lower slip, leading to conservative global predictions.

Despite this simplification, the analytical model successfully captures non-linearity onset and progression. Accuracy could be enhanced through a multi-segment iterative scheme accounting for varying connection stiffness along the span.

Structural Interpretation and Serviceability Limits

The numerical model's high accuracy, based on the mean Foschi law, suggests the presence of a smoothing effect within the composite assembly. In this context, the global response appears to be governed by the statistical mean behaviour of the fasteners rather than by individual extremes. However, this observation is derived from a limited experimental dataset and a single beam configuration and should therefore be considered as a tendency rather than a general conclusion.

The global structural behaviour can be divided into three distinct phases (Appendix 6.2.7). Phase 1 corresponds to the initial linear response where connectors remain undamaged. Phase 2 is characterised by progressive connector damage, resulting in gradual stiffness degradation. In Phase 3, connectors no longer contribute to the assembly's stiffness, and the beam behaves as a layered system without connection.

Accounting for connection non-linearity is essential to identify irreversible damage onset. While standard serviceability limits ($L/250$) are intended to ensure elastic behaviour, the tested beams exhibited an early-onset non-linear response before reaching this threshold. Although consistently observed across the three specimens, this result should be interpreted cautiously and confirmed through additional experimental investigations. It nevertheless highlights a specific behavioural trend that warrants further exploration regarding the relevance of conventional serviceability criteria for such systems.

4.3 Structural Efficiency of the Beam with Densified Wooden Nails

Two primary metrics can be used to evaluate the structural efficiency of the composite beam. The effective bending stiffness $(\mathrm{EI})_{\mathrm{eff}}$ is derived from the mid-span deflection using the elastic relationship expressed in Eq. (3). The relative gain (G) is used to quantify the degree of composite action, Eq. (4).

$$(EI)_{eff} = PL^3/(48\, w_{mid-span}) \tag{3}$$

$$G = \frac{(EI)_{eff} - (EI)_0}{(EI)_\infty - (EI)_0} \tag{4}$$

where:
$(EI)_\infty$: bending stiffness of fully composite section
$(EI)_0$: bending stiffness of non-composite section

Table 8 summarises the effective bending stiffness $(\mathrm{EI})_{\mathrm{eff}}$ and the corresponding stiffness gain G at different load levels. When approximately 10 % of the maximum load is applied, the investigated beam configuration exhibits an initial stiffness gain of about 30 %. However, this gain decreases progressively as loading increases, reaching approximately 20 % at the conventional serviceability limit ($L/250$) and about 10 % under severe service conditions ($L/100$). While these trends are consistently observed across all tested beams (Appendix 6.2.8, Table 12), they remain specific to the tested configuration.

For comparison purposes, Table 8 includes benchmark with a fully composite (glued) solution and alternative connection systems using 12 mm wooden dowels. These alternative systems exhibit a predominantly linear structural response in comparable configurations [65], [66], [67].

Despite their small diameter, densified wooden nails demonstrated a meaningful stiffness gain within the specific parameters of this study (connector spacing s = 65 mm) and offer practical advantages compared to dowel systems, including faster assembly and the absence of pre-drilling. However, within this specific configuration, their structural performance in the tested configuration is strongly governed by connection non-linearity, which limits stiffness gains as load increases. These observations should be further investigated for other beam geometries and loading conditions to assess their general applicability.

		$EI_{K=0}$ [kNm²]	$EI_{K=\infty}$ [kNm²]	$(EI)_{eff,\,exp}$ [kNm²]	G_{exp} [%]	$(EI)_{eff,\,dowels}$ [kNm²]	G_{dowels} [%]
BEAM 1	$0.1\,F_{max}$	17.43	464.68	160.37	32.0%	144.78	28.5%
	$F_{L/250}$			110.32	20.8%		
	$F_{L/100}$			70.00	11.8%		

Table 8 - BEAM 1: $(EI)_{eff}$ and G values at serviceability levels. Theoretical DLT solution (Φ12mm, s=65mm) for comparison.

5. CONCLUSIONS

Connection Stiffness

- The slip modulus values obtained experimentally and the ETA-based formulation showed strong agreement.
- Eurocode 5 significantly underestimated the initial stiffness of the densified wooden fasteners, highlighting the need for specific design frameworks for such innovative connectors.
- The mechanical behaviour observed in the single-fastener shear tests revealed a non-linear behaviour that was successfully captured using the Foschi law.

Modelling aspects

The results highlight the importance of considering the non-linear connection behaviour to predict the structural response of timber beams assembled with densified wooden nails for the investigated configurations.

- The non-linear finite element model (FEM) provided the most accurate predictions among the tested models, as it captures the redistribution of loads between connectors and variation in connection stiffness along the span.
- Within the linear-elastic regime, the Generalised Girhammar analytical solution provides identical results to the finite element simulations, supporting its applicability for multi-layered systems.
- When extended to non-linear behaviour via a secant stiffness approach, the analytical model tends to overestimate deformations, due to the simplifying assumption of a uniform connection stiffness along the interface.

Structural Performance and Interpretation

While the following observations are derived from a limited number of tested beam, the consistency of the experimental responses suggests consistent behavioural trends for the investigated configuration. These findings highlight the need for further investigation into the implications of early-onset non-linearity on serviceability assessment and design practice:

- For the tested laminated beam configuration, the experimental results reveal a pronounced non-linear and ductile response. While the two beams tested up to failure exhibited high ductility ratios, the associated structural stiffness decreases rapidly as loading progresses.
- A key observation from the investigated specimens is that non-linear behaviour develops before conventional serviceability limits (L/250) are reached.
- The global beam response is shown to be closely aligned with the non-linear modelling based on the *mean* connection behaviour. This indicates a potential smoothing effect within the redundant fastener system, where the structural response is governed by the mean connector behaviour rather than by local extremes.

Perspectives for Future Research

The findings suggest several perspectives for further investigations based on these initial results:

- *Analytical Refinement:* Development of advanced analytical formulations taking into account spatially varying stiffness to approach FE precision while maintaining computational speed.
- *Long-term Durability:* Assessment of the system's performance under sustained loads (creep) or load cycles and fluctuating environmental conditions (moisture cycles).
- *Reliability-based Design:* Investigating serviceability criteria suited to timber–timber connections exhibiting early non-linearity, to support the safe and realistic design of such fastener systems.

6. APPENDICES

6.1 Densified Wooden Nail Joint

6.1.1 Single shear tests

	ρ [kg/m³]	RH [%]	EXP – F_v [N]	EC5 – F_v [N]	EC5 – K_{ser} [N/mm]	ETA– F_v [N]	ETA – K_{ser} [N/mm]
SAP - CIS - 1	a. 452 b. 470	7.5 (±0.4)	1061.62	935.17 (f. mode)	1634.56	809.88	2699.61
SAP - CIS - 2	a. 447 b. 460	7.5 (±0.4)	1180.59	927.32 (f. mode)	1593.38	803.09	2676.95
SAP - CIS - 3	a. 439 b. 457	7.5 (±0.4)	1388.28	921.54 (f. mode)	1564.18	798.08	2660.26
SAP - CIS - 4	a. 447 b. 456	7.5 (±0.4)	1060.54	925.1 (f. mode)	1581.68	801.16	2670.54
SAP - CIS - 5	a. 448 b. 449	7.5 (±0.4)	1258.39	922.3 (f. mode)	1567.09	798.73	2662.44
SAP - CIS - 6	a. 477 b. 450	7.5 (±0.4)	1313.54	937.21 (f. mode)	1646.39	811.65	2705.49
SAP - CIS - 7	a. 454 b. 463	7.5 (±0.4)	1119.43	933.05 (f. mode)	1622.76	808.04	2693.47
SAP - CIS - 8	a. 457 b. 477	7.5 (±0.4)	1270.89	940.75 (f. mode)	1664.19	814.71	2715.71
SAP - CIS - 9	a. 440 b. 484	7.5 (±0.4)	1218.21	935.39 (f. mode)	1640.47	810.07	2700.24
SAP - CIS - 10	a. 446 b. 444	7.5 (±0.4)	1278.77	918.86 (f. mode)	1549.65	795.76	2652.52
SAP - CIS - 11	a. 513 b. 540	9.3 (±0.3)	1155.08	999.31 (f. mode)	1646.39	865.42	2884.75
SAP - CIS - 12	a. 524 b. 516	9.3 (±0.3)	1155.08	993.24 (f. mode)	1664.19	860.17	2867.25
SAP - CIS - 13	a. 528 b. 503	9.3 (±0.3)	1337.27	988.75 (f. mode)	1640.47	856.28	2854.27
SAP - CIS - 14	a. 539 b. 501	9.3 (±0.3)	1369.47	992.62 (f. mode)	1549.65	859.64	2865.46
SAP - CIS - 15	a. 516 b. 499	9.3 (±0.3)	1437.03	980.87 (f. mode)	1995.25	849.46	2831.52
SAP - CIS - 16	a. 519 b. 480	9.3 (±0.3)	1355.88	972.71 (f. mode)	1995.25	842.39	2807.98
SAP - CIS - 17	a. 457 b. 456	9.3 (±0.3)	1494.64	930.26 (f. mode)	1957.48	805.63	2685.43
SAP - CIS - 18	a. 486 b. 451	9.3 (±0.3)	1538.96	942.01 (f. mode)	1957.48	815.8	2719.34
SAP - CIS - 19	a. 447 b. 492	9.3 (±0.3)	1551.66	942.65 (f. mode)	1932.44	816.36	2721.19
SAP - CIS - 20	a. 437 b. 469	9.3 (±0.3)	1294.43	926.27 (f. mode)	1932.44	802.17	2673.91
SAP - CIS - 21	a. 493 b. 438	9.3 (±0.3)	1422.36	938.17 (f. mode)	1957.48	812.48	2708.26
SAP - CIS - 22	a. 477 b. 450	9.3 (±0.3)	1416.06	937.21 (f. mode)	1957.48	811.65	2705.49

SAP - CIS - 23	a. 457 b. 477	9.3 (±0.3)	919.76	940.75 (f. mode)	1885.78	814.71	2715.71
SAP - CIS - 24	a. 440 b. 484	9.3 (±0.3)	1507.45	935.39 (f. mode)	1885.78	810.07	2700.24
SAP - CIS - 25	a. 446 b. 444	9.3 (±0.3)	1015.73	918.86 (f. mode)	1842.57	795.76	2652.52
SAP - CIS - 26	a. 513 b. 540	9.3 (±0.3)	1104.46	999.31 (f. mode)	1608.05	865.42	2884.75
SAP - CIS - 27	a. 524 b. 516	9.3 (±0.3)	1124.85	993.24 (f. mode)	1673.11	860.17	2867.25
SAP - CIS - 28	a. 528 b. 503	9.3 (±0.3)	1308.02	988.75 (f. mode)	1679.07	856.28	2854.27
SAP - CIS - 29	a. 539 b. 501	9.3 (±0.3)	1234.85	992.62 (f. mode)	1679.07	859.64	2865.46
SAP - CIS - 30	a. 516 b. 499	9.3 (±0.3)	1324.86	980.87 (f. mode)	1590.45	849.46	2831.52
SAP - CIS - 31	a. 447 b. 492	9.3 (±0.3)	1069.01	942.65 (f. mode)	1590.45	816.36	2721.19
SAP - CIS - 32	a. 437 b. 469	9.3 (±0.3)	1246.47	926.27 (f. mode)	1658.25	802.17	2673.91
SAP - CIS - 33	a. 493 b. 438	9.3 (±0.3)	991.31	938.17 (f. mode)	1658.25	812.48	2708.26
mean	477.98	7.5 or 9.3	1258.33	951.44	1727.31	823.97	2746.58
standard dev.	31.78	0.4 or 0.3	162.57	27.88	153.96	24.14	80.47
cov	6.7%	5.4% or 3.6%	12.9%	2.9%	8.9%	2.9%	2.9%

Table 9 - Single shear tests specimens - Data & Results.

6.1.2 Experimental stiffness

ISO 6891:1983

$$K_{ser} = \frac{0.4F_{est}}{v_{i,mod}} \tag{5}$$

$$v_{i,mod} = \frac{4}{3}(v_{04} - v_{01}) \tag{6}$$

where:
$v_{i,mod}$: modified initial slip;
v_{04}: displacement corresponding to $0.4F_{est}$;
v_{01}: displacement corresponding to $0.1F_{est}$.

6.1.3 Analytical predicted values

EC5

$$F_{v,Rk} = \min \begin{cases} a.)\ f_{h,1,k} \cdot t_{h1} \cdot d \\ b.)\ f_{h,2,k} \cdot t_{h2} \cdot d \\ c.)\ \dfrac{f_{h,1,k} \cdot t_{h1} \cdot d}{1+\beta}\left[\sqrt{\beta + 2\beta^2\left[1 + \dfrac{t_{h2}}{t_{h1}} + \left(\dfrac{t_{h2}}{t_{h1}}\right)^2\right] + \beta^3\left(\dfrac{t_{h2}}{t_{h1}}\right)^2} - \beta\left(1 + \dfrac{t_{h2}}{t_{h1}}\right)\right] \\ d.)\ 1.05\dfrac{f_{h,1,k} \cdot t_{h1} . d}{2+\beta}\left[\sqrt{2\beta(1+\beta) + \dfrac{4\beta \cdot (2+\beta) \cdot M_{y,k}}{f_{h,1,k} \cdot d \cdot {t_{h1}}^2}} - \beta\right] \\ e.)\ 1.05\dfrac{f_{h,1,k} \cdot t_{h2} \cdot d}{1+2\beta}\left[\sqrt{2\beta^2(1+\beta) + \dfrac{4\beta \cdot (1+2\beta) \cdot M_{y,k}}{f_{h,1,k} \cdot d \cdot {t_{h2}}^2}} - \beta\right] \\ f.)\ 1.15\sqrt{\dfrac{2\beta}{1+\beta}}\sqrt{2M_{y,k} \cdot f_{h,1,k} \cdot d} \end{cases} \tag{7}$$

with:

$$\beta = \frac{f_{h,2,k}}{f_{h,1,k}}$$

where:
$f_{h,1,k}, f_{h,2,k}$: characteristic embedment strengths of members 1 and 2;
$t_{h,1}, t_{h,2}$: embedment depths of members 1 and 2;
$M_{y,k}$: characteristic yield moment (from [36]);
d: diameter of the fastener.

$$K_{ser} = \rho_{mean}^{1.5} \cdot d^{0.8}/23 \tag{8}$$

where:
ρ_{mean}: mean density, in [kg/m³];
d: diameter of the fastener, in [mm].

ETA

$$F_{v,Rk} = \sqrt{\frac{2\beta}{1+\beta}}\sqrt{1.5M_{y,k} \cdot f_{h,1,k} \cdot d} \cdot min\begin{cases} 1 \\ t_1/t_{1,req} \\ t_2/t_{2,req} \end{cases} \tag{9}$$

with:
$t_{1,req} = \left(\sqrt{\frac{\beta}{1+\beta}} + 1\right) \cdot \sqrt{\frac{4M_{y,k}}{0.75 \cdot f_{h,1,k} \cdot d}}$ and $t_{2,req} = \left(\sqrt{\frac{1}{1+\beta}} + 1\right) \cdot \sqrt{\frac{4M_{y,k}}{0.75 \cdot f_{h,2,k} \cdot d}}$

where:
$M_{y,k}$: characteristic yield moment;
$t_{1,req}$, $t_{2,req}$: required thickness of members 1 and 2.

$$K_{ser} = \frac{F_{v,Rk}}{0.3\ mm} \tag{10}$$

6.2 Composite Beam

6.2.1 Numerical modelling – Mesh sensitivity analysis

Evolution of the vertical displacement at midspan for a load of 4.84 kN (linear model - K_{ser}) for specimen BEAM 2 is given in Table 10.

	Number of mesh elements per layer [-]				
	87	348	780	***3120***	12480
w_{NUM} [mm]	12.240	12.245	12.248	***12.248***	12.248

Table 10 - Mesh sensitivity analysis

6.2.2 Analytical modelling – Non-linear analytical procedure

The non-linear analytical response of the composite beam is obtained through an iterative secant-stiffness approach. The objective is to account for the non-linear load-slip behaviour of the connectors while maintaining the analytical framework.

Initialisation

The procedure starts from a linear-elastic solution of the beam using an initial connector stiffness. This initial value corresponds to the linear stiffness derived from the connector characterisation (Section 2), ensuring a consistent initial condition.

Iterative scheme

At each iteration, the following steps are performed:

- *Beam resolution:* The beam response is computed using the Girhammar Generalised Exact Method. This provides the global deflection $w(x)$ and the longitudinal displacements $u_i(x)$ of each lamella.
- *Slip evaluation:* The relative slip at each interface is calculated along the beam length. For each interface, a representative slip value is extracted. In this study, the maximum local slip is used to update the stiffness, leading to a conservative estimate of connection degradation.
- *Stiffness update:* The connector force is computed using the calibrated Foschi constitutive law, and an equivalent secant stiffness is derived as: $k_i = \frac{F(\delta_i)}{\delta_i}$. This stiffness is assumed uniform along each interface, which is a key simplifying assumption of the analytical model.
- *Relaxation (stabilisation):* To ensure numerical stability, a relaxation scheme is applied: $k_i^{(new)} = \alpha k_i^{(updated)} + (1-\alpha) k_i^{(old)}$ where α is a relaxation factor (typically between 0.5 and 0.9).
- *Convergence check:* Convergence is evaluated based on the relative variation of the global deflection $w(x)$ and longitudinal displacements $u_i(x)$. The iteration is considered converged when: $\max\left(\frac{|w^{(n)}-w^{(n-1)}|}{|w^{(n)}|}, \frac{|u^{(n)}-u^{(n-1)}|}{|u^{(n)}|}\right) < \varepsilon$ with a tolerance $\varepsilon = 10^{-6}$.

Convergence behaviour

In practice, convergence is typically achieved within 10 to 30 iterations, depending on the load level and degree of non-linearity.

Limitations

The main limitation of the approach lies in the assumption of a single uniform stiffness per interface, derived from a representative slip value. This simplification neglects the spatial variability of slip and stiffness along the beam. As a result, the local stiffness degradation is not fully captured, and the model tends to overestimate global deflections.

6.2.3 Analytical modelling – Load in connectors at interfaces

Figure 7 illustrates the evolution of the connector loads at the interface between layers 3 and 4 for both three-point and four-point bending configurations. The results clearly show that fastener loads are non-uniform along the beam, particularly in the four-point bending case, where the presence of a constant bending moment region leads to reduced loading of connectors. This heterogeneity is less pronounced in the three-point bending configuration adopted in this study.

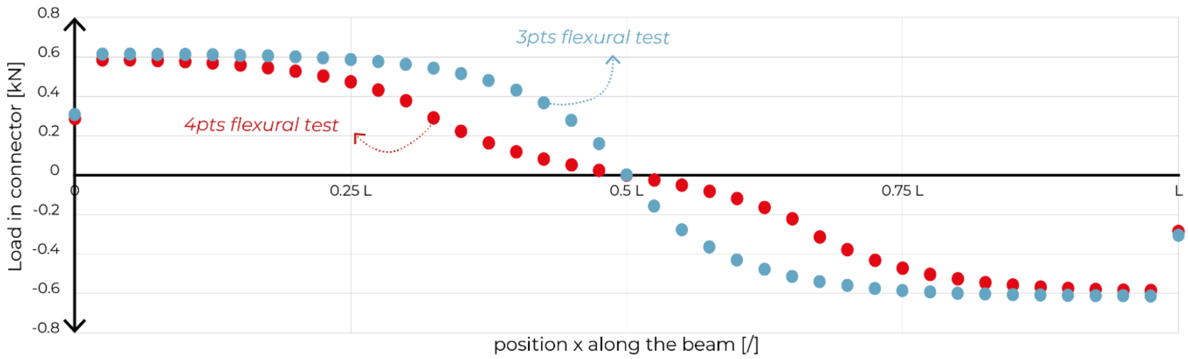

Figure 7 - Evolution of connector loads along the beam at the interface of layers 3 and 4 - (blue= three-point bending test; red=4point bending test).

6.2.4 Experimental tests

MOE – Four-point bending tests

The modulus of elasticity (MOE) was determined through four-point bending tests according to a localised measurement protocol as illustrated in Figure 8.

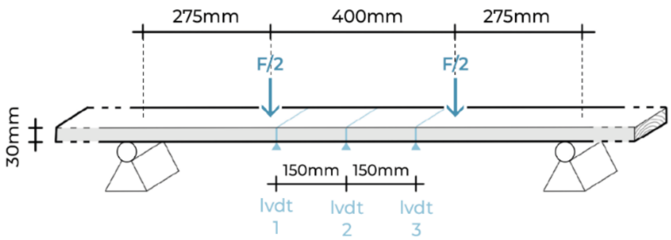

Figure 8 - Four-point bending setup for lamella MOE measurement.

6.2.5 BEAM 0 - Results

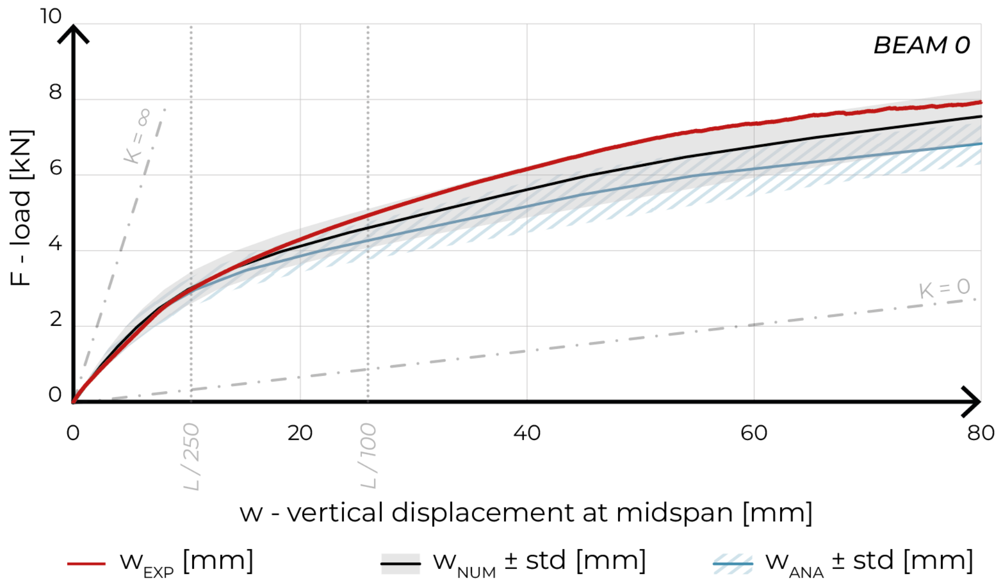

Figure 9 - BEAM 0: Experimental and non-linear models' predictions with variation range. Dashed lines: limit behaviours (K=∞, K=0).

6.2.6 BEAM 2 - Results

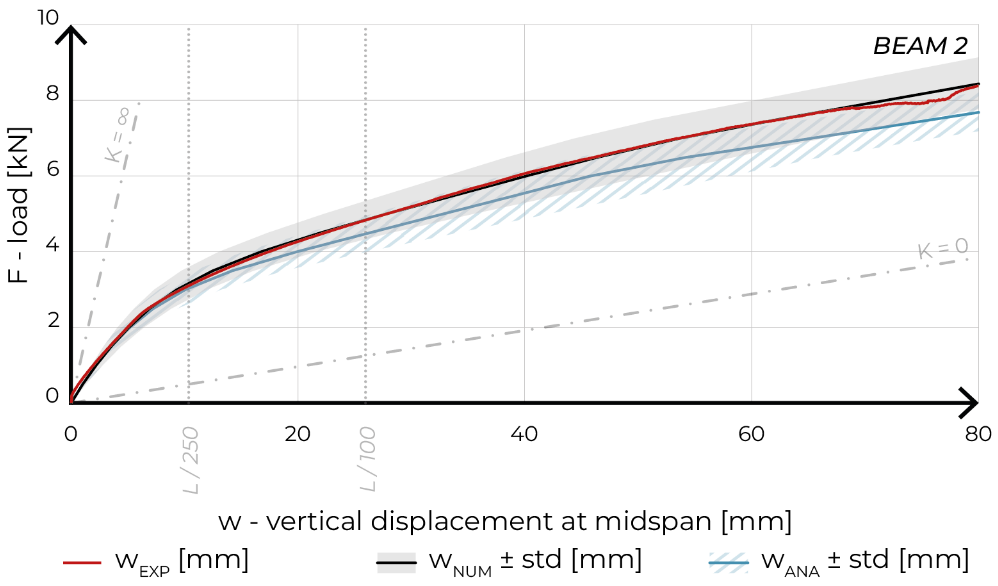

Figure 10 - BEAM 2: Experimental and non-linear models' predictions with variation range. Dashed lines: limit behaviours (K=∞, K=0).

6.2.7 BEAM 1 – Linear approximation

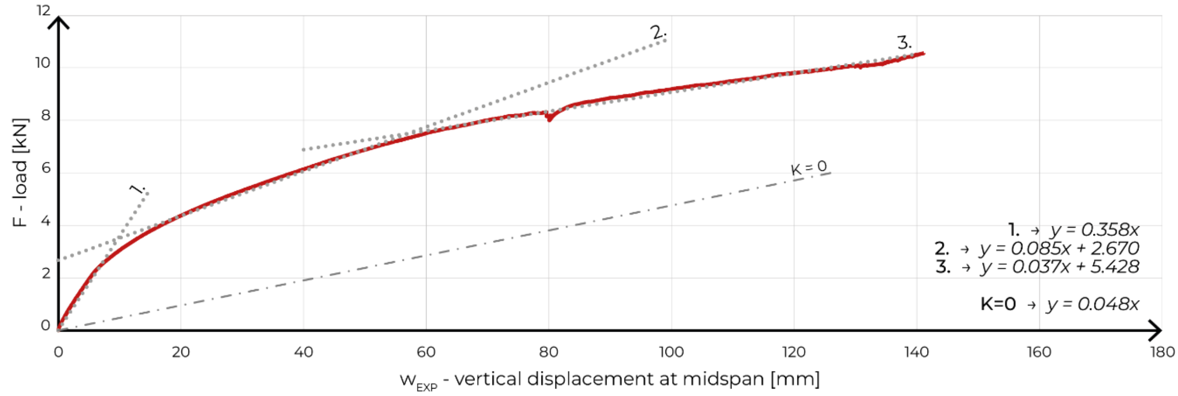

Figure 11 - BEAM 1 – EXP: Linear approximation

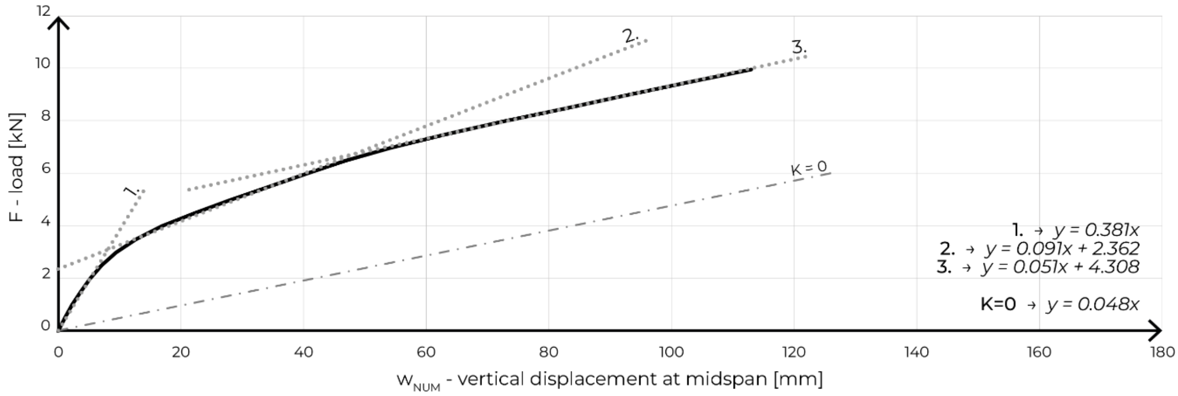

Figure 12 - BEAM 1 – NUM: Linear approximation

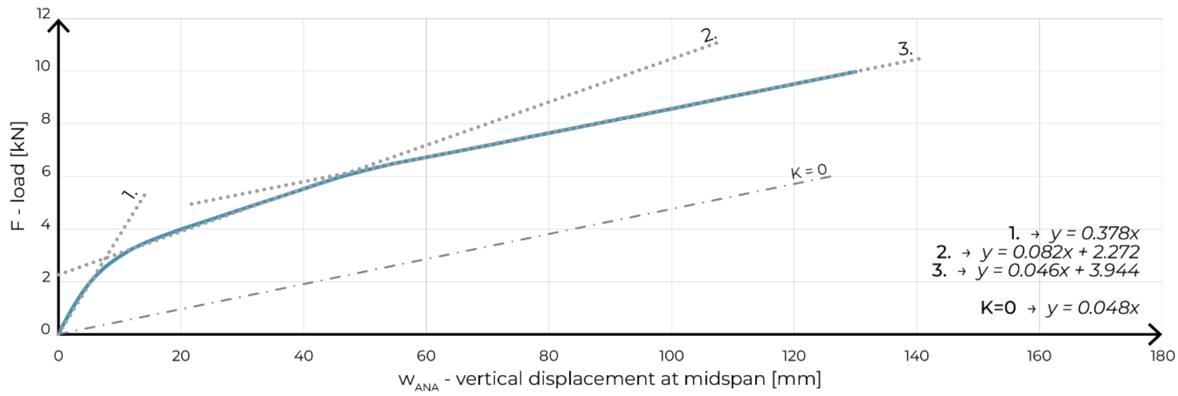

Figure 13 - BEAM 1 – ANA: Linear approximation

6.2.8 All Beams Results

	BEAM 0		BEAM 1		BEAM 2	
	$F_{L/250}$	$F_{L/100}$	$F_{L/250}$	$F_{L/100}$	$F_{L/250}$	$F_{L/100}$
load [kN]	3.00	4.96	3.12	4.98	3.11	4.84
w_{exp} [mm]	10.40	26.00	10.40	26.00	10.40	26.00
$w_{ANA\_K.exp}$ [mm]	12.17 (*+17.0%*)	20.10 (*-22.7%*)	11.76 (*+13.1%*)	18.73 (***-27.9%***)	11.62 (*+11.7%*)	18.10 (***-30.4%***)
$w_{NUM\_K.exp}$ [mm]	12.18 (*+17.1%*)	20.11 (*-22.7%*)	11.77 (*+13.1%*)	18.74 (***-27.9%***)	11.62 (*+11.8%*)	18.11 (***-30.4%***)
$w_{NUM\_K.EC5}$ [mm]	17.06 (***+64.0%***)	28.17 (*+8.4%*)	15.96 (***+53.5%***)	25.42 (*-2.2%*)	15.79 (***+51.8%***)	24.60 (*-5.4%*)
$w_{NUM\_K.ETA}$ [mm]	12.21 (*+17.4%*)	20.17 (*-22.4%*)	11.80 (*+13.5%*)	18.80 (***-27.7%***)	11.66 (*+12.1%*)	18.16 (***-30.1%***)
w_{ANA_NL} [mm]	10.77 (*+3.6%*)	36.32 (***+39.7%***)	10.19 (*-2.0%*)	30.51 (*+17.3%*)	10.03 (*-3.6%*)	28.58 (*+9.9%*)
w_{NUM_NL} [mm]	10.09 (*-3.0%*)	30.46 (*+17.1%*)	10.09 (*-3.0%*)	27.70 (*+6.6%*)	9.93 (*-4.6%*)	25.90 (*-0.4%*)

Table 11 - All beams: Model deflections at serviceability levels. Relative error (%) vs. experimental reference.

	BEAM 0			BEAM 1			BEAM 2		
	$0.1\ F_{max}$	$F_{L/250}$	$F_{L/100}$	$0.1\ F_{max}$	$F_{L/250}$	$F_{L/100}$	$0.1\ F_{max}$	$F_{L/250}$	$F_{L/100}$
EI_0 [kNm²]	12.63			17.43			17.61		
EI_∞ [kNm²]	351.49			464.68			484.35		
$(EI)_{eff,\ exp}$ [kNm²]	131.12	105.61	69.72	160.37	110.32	70.00	177.46	109.00	68.29
G_{exp} [%]	35.0%	27.4%	16.8%	32.0%	20.8%	11.8%	34.2%	19.6%	10.9%
$(EI)_{eff,\ dowels}$ [kNm²]	132.07			144.78			146.31		
G_{dowels} [%]	35.2%			28.5%			27.6%		

Table 12 - All beams: $(EI)_{eff}$ and G values at serviceability levels. Theoretical DLT solution (Φ12mm, s=65mm) for comparison.

7. REFERENCES

[1] Global ABC and UNEP, ‘2022 Global Status Report for Buildings and Construction: Towards a Zero-emission, Efficient and Resilient Buildings and Construction Sector’, 2022. Accessed: Jan. 16, 2025. [Online]. Available: https://globalabc.org/resources/publications/2022-global-status-report-buildings-and-construction

[2] L. Orozco *et al.*, ‘Advanced Timber Construction Industry: A Quantitative Review of 646 Global Design and Construction Stakeholders’, *Buildings*, vol. 13, no. 9, Art. no. 9, Sep. 2023, doi: 10.3390/buildings13092287.

[3] H. Huang, S. Su, and L. Li, ‘Advancing timber construction: historical growth, research frontiers, and time series forecasting’, *Journal of Asian Architecture and Building Engineering*, vol. 0, no. 0, pp. 1–30, Jul. 2024, doi: 10.1080/13467581.2024.2373829.

[4] L. Tupenaite, L. Kanapeckiene, J. Naimaviciene, A. Kaklauskas, and T. Gecys, ‘Timber Construction as a Solution to Climate Change: A Systematic Literature Review’, *Buildings*, vol. 13, no. 4, Art. no. 4, Apr. 2023, doi: 10.3390/buildings13040976.

[5] S. C. Thomas and A. R. Martin, ‘Carbon Content of Tree Tissues: A Synthesis’, *Forests*, vol. 3, no. 2, Art. no. 2, Jun. 2012, doi: 10.3390/f3020332.

[6] M. Gong, ‘Wood and Engineered Wood Products: Stress and Deformation’, in *Engineered Wood Products for Construction*, M. Gong, Ed., IntechOpen, 2022. doi: 10.5772/intechopen.101199.

[7] R. Yadav and J. Kumar, ‘Engineered Wood Products as a Sustainable Construction Material: A Review’, in *Engineered Wood Products for Construction*, M. Gong, Ed., IntechOpen, 2022. doi: 10.5772/intechopen.99597.

[8] I. Jahan, G. Zhang, M. Bhuiyan, and S. Navaratnam, ‘Circular Economy of Construction and Demolition Wood Waste—A Theoretical Framework Approach’, *Sustainability*, vol. 14, no. 17, Art. no. 17, Jan. 2022, doi: 10.3390/su141710478.

[9] B. Lesar, M. Humar, and G. Hora, ‘Quality assessment of recycled wood with and without non-wooden materials from selected recycling companies in Europe’, *Waste Management*, vol. 79, pp. 362–373, Sep. 2018, doi: 10.1016/j.wasman.2018.08.002.

[10] U. Mantau, ‘Wood flow analysis: Quantification of resource potentials, cascades and carbon effects’, *Biomass and Bioenergy*, vol. 79, pp. 28–38, Aug. 2015, doi: 10.1016/j.biombioe.2014.08.013.

[11] M. Vis, U. Mantau, and B. Allen, Eds, ‘Study on the optimised cascading use of wood’, Publications Office, Brussels (Belgium), Final report No 394/PP/ENT/RCH/14/7689, 2016. doi: 10.2873/827106.

[12] N. Ahn, A. Dodoo, M. Riggio, L. Muszynski, L. Schimleck, and M. Puettmann, ‘Circular economy in mass timber construction: State-of-the-art, gaps and pressing research needs’, *Journal of Building Engineering*, vol. 53, p. 104562, Aug. 2022, doi: 10.1016/j.jobe.2022.104562.

[13] M. Ghobadi and S. M. E. Sepasgozar, ‘Circular economy strategies in modern timber construction as a potential response to climate change’, *Journal of Building Engineering*, vol. 77, p. 107229, Oct. 2023, doi: 10.1016/j.jobe.2023.107229.

[14] M. Conway, S. Mehra, A. M. Harte, and C. O’Ceallaigh, ‘Densified wood dowel reinforcement of timber perpendicular to the grain: a pilot study’, *Journal of Structural Integrity and Maintenance*, vol. 6, no. 3, pp. 177–186, Jul. 2021, doi: 10.1080/24705314.2021.1906090.

[15] M. Derikvand and D. B. Khoshroodi, ‘Experimental and analytical evaluation of shear capacity of reclaimed timber connections with thermo-mechanically densified wooden dowels’, *Construction and Building Materials*, vol. 504, p. 144613, Dec. 2025, doi: 10.1016/j.conbuildmat.2025.144613.

[16] L. Han, A. Kutnar, J. Sandak, I. Šušteršič, and D. Sandberg, ‘Adhesive-and Metal-Free Assembly Techniques for Prefabricated Multi-Layer Engineered Wood Products: A Review on Wooden Connectors’, *Forests*, vol. 14, no. 2, Art. no. 2, Feb. 2023, doi: 10.3390/f14020311.

[17] A. Sotayo *et al.*, ‘Review of state of the art of dowel laminated timber members and densified wood materials as sustainable engineered wood products for construction and building applications’, *Developments in the Built Environment*, vol. 1, p. 100004, Feb. 2020, doi: 10.1016/j.dibe.2019.100004.

[18] European Committee for Standardization, *EN 1995-1-1:2025: Eurocode 5: Design of timber structures - Part 1-1: General rules and rules for buildings*, Brussels (Belgium)., Nov. 20, 2025.
[19] I. U. Khan, M. Subhani, K. Ghabraie, and M. Ashraf, 'Mechanical performance and design challenges of wooden fasteners: a critical analysis of evaluation methods and standards', *Eur. J. Wood Prod.*, vol. 83, no. 4, p. 143, Jul. 2025, doi: 10.1007/s00107-025-02293-1.
[20] RAIMUND BECK NAGELTECHNIK GmbH, 'LIGNOLOC® Wooden Nail System',
[21] M. Inoue, K. Adachi, and K. Kamachi, 'Development of wooden-based nails for wooden pallet', in *Proceedings of the International Convention of Society of Wood Science and Technology and United Nations Economic Commission for Europe – Timber Committee*, Geneva (Switzerland), 2010.
[22] M. Alvarez *et al.*, 'The Buga Wood Pavilion : Integrative Interdisciplinary Advancements of Digital Timber Architecture', in *Paper Proceedings of the 39th Annual Conference of the Association for Computer Aided Design in Architecture*, Austin (Texas - USA), 2019.
[23] 'Woodbloc: The glue-free connected solid wood wall', Woodbloc. Accessed: Jan. 27, 2026. [Online]. Available: https://woodbloc.de/en/
[24] T. Rockenschaub, *European Technical Assessment ETA-24/0946 - Woodbloc Massivholzwand*, Nov. 22, 2024.
[25] S. Wang *et al.*, 'Hysteretic response and analytical modeling of a novel adhesive-free Wooden-Nail Cross-Laminated Timber (WNCLT) shear wall', *Journal of Building Engineering*, vol. 120, p. 115474, Feb. 2026, doi: 10.1016/j.jobe.2026.115474.
[26] S. Wang *et al.*, 'Lateral resistance performance of wood-frame shear walls with wooden nail connections: Experimental and finite element analysis', *Journal of Bioresources and Bioproducts*, vol. 10, no. 3, pp. 410–424, Aug. 2025, doi: 10.1016/j.jobab.2025.04.002.
[27] G. Ruan, G. Filz, and G. Fink, 'Planar rectangular, slide-in reciprocal frame structures using salvaged timber and wooden nails', in *Proceedings of the IASS 2022 Symposium affiliated with APCS 2022 conference*, Beijing (China), Sep. 2022.
[28] G. Ruan, 'Timber-only Structures & Architecture – Exploring the Potential of Using Salvaged Timber and Wooden Nails', 2024.
[29] M. Riggio, D. Pauliny, J. Sandak, and A. Sandak, 'Novel Nail-Like Wood Connectors', *Advanced Materials Research*, vol. 778, pp. 647–654, Sep. 2013, doi: 10.4028/www.scientific.net/AMR.778.647.
[30] M. Riggio, J. Sandak, and A. Sandak, 'Densified wooden nails for new timber assemblies and restoration works: A pilot research', *Construction and Building Materials*, vol. 102, Jun. 2015, doi: 10.1016/j.conbuildmat.2015.06.045.
[31] H. Hasan, A. Reddy, and A. Tsayjacobs, 'Robotic Fabrication of Nail Laminated Timber', in *2019 Proceedings of the 36th ISARC, Banff, Canada*, Banff (Canada), May 2019. doi: 10.22260/ISARC2019/0162.
[32] G. Ruan, G. H. Filz, and G. Fink, 'Shear capacity of timber-to-timber connections using wooden nails', *Wood Material Science & Engineering*, vol. 17, no. 1, pp. 20–29, Jan. 2022, doi: 10.1080/17480272.2021.1964595.
[33] S. Wang *et al.*, 'Mechanical behavior and theoretical modeling of wooden nails under various stress conditions', *Construction and Building Materials*, vol. 458, p. 139624, Jan. 2025, doi: 10.1016/j.conbuildmat.2024.139624.
[34] V. Aleksiievets *et al.*, 'Performance of nail joints of wooden structural elements under low-cycle loads', in *Procedia Structural Integrity*, in VIII International Conference "In-service Damage of Materials: Diagnostics and Prediction" (DMDP 2025), vol. 81. Jan. 2026, pp. 422–429. doi: 10.1016/j.prostr.2026.03.073.
[35] N. Le Thuy, T. T. Tran, T. T. Thuy Van, N. Hong Son, N. T. Hanh, and N. Hoang Anh, 'Numerical Modelling of Densified Wooden Nails in Timber Assemblies Using Abaqus', in *4th International Conference on Structural Health Monitoring and Engineering Structures (SHM&ES 2025)*, L. T. Cuong, N. Fantuzzi, R. Capozucca, V. T. B. Quyen, and S. Khatir, Eds, Cham: Springer Nature Switzerland, 2026, pp. 871–879. doi: 10.1007/978-3-032-04645-1_101.

[36] T. Bruun, *European Technical Assessment ETA-23/0041 - LignoLoc® wood-based dowel type fasteners*, Mar. 27, 2023.
[37] International Standard, *ISO 6891:1992: Timber structures - Joints made with mechanical fasteners - General principles for the determination of strength and deformation characteristics (ISO 6891:1983)*, Brussels (Belgium)., Jun. 23, 1992.
[38] R. O. Foschi and T. Bonac, 'Load-Slip Characteristics for Connections With Common Nails', *Wood Science*, vol. 9, no. 3, pp. 118–123, Jan. 1977.
[39] 'LIGNOLOC® clous en bois | Beck Fastening'. Accessed: Jan. 27, 2026. [Online]. Available: https://www.beck-fastening.com/fr/innovation/lignoloc
[40] RAIMUND BECK NAGELTECHNIK GmbH, 'Collated wooden nails', Feb. 2019.
[41] S. Wang *et al.*, 'Eco-friendly wooden nails: Bonding mechanisms and withdrawal resistance in sustainable timber connections', *Journal of Cleaner Production*, vol. 486, p. 144606, Jan. 2025, doi: 10.1016/j.jclepro.2024.144606.
[42] Y. Bai and Y. Xiao, 'Withdrawal capacity of wooden nails in glubam', *Construction and Building Materials*, vol. 523, p. 146269, May 2026, doi: 10.1016/j.conbuildmat.2026.146269.
[43] C. Gerber, K. Collado, and J. J. Morrell, 'Impact of moisture cycling on lateral resistance of resin-impregnated compressed beech nails in radiata pine timber', *International Wood Products Journal*, vol. 12, no. 3, pp. 147–151, Jul. 2021, doi: 10.1080/20426445.2021.1906389.
[44] S. Wang, F. Wang, F. Kong, P. Ma, Z. Chen, and Z. Que, 'Influence of repeated wetting and drying on withdrawal capacity of wooden nails and metal nails', *Construction and Building Materials*, vol. 409, p. 133991, Nov. 2023, doi: 10.1016/j.conbuildmat.2023.133991.
[45] European Committee for Standardization, *EN 384:2016+A2:2022 Structural timber - Determination of characteristic values of mechanical properties and density*, Brussels (Belgium)., Jun. 11, 2022.
[46] European Committee for Standardization, *EN 13183-1:2002: Moisture content of a piece of sawn timber - Part 1 Determination by oven dry method*, Brussels (Belgium)., Jun. 28, 2002.
[47] C. Pirazzi, 'Zur Berechnung von Holzschalen in Brettrippenbauweise mit elastischem Verbundquerschnitt', EPFL, Lausanne, 2005. doi: 10.5075/epfl-thesis-3229.
[48] L. Resch, 'Développement d'éléments de construction en bois de pays lamellés assemblés par tourillons thermo-soudés', These de doctorat, Nancy 1, 2009. Accessed: Nov. 21, 2023. [Online]. Available: https://www.theses.fr/2009NAN10142
[49] A. M. P. G. Dias, 'Analysis of the Nonlinear Behavior of Timber-Concrete Connections', *J. Struct. Eng.*, vol. 138, no. 9, pp. 1128–1137, Sep. 2012, doi: 10.1061/(ASCE)ST.1943-541X.0000523.
[50] H. J. Blaß and C. Sandhaas, 'E1. Joints in timber structures', in *Timber engineering: principles for design*, Karlsruhe: KIT Scientific Publishing, 2017.
[51] M. Domínguez *et al.*, 'Structural Timber Connections with Dowel-Type Fasteners and Nut-Washer Fixings: Mechanical Characterization and Contribution to the Rope Effect', *Materials*, vol. 15, no. 1, Dec. 2021, doi: 10.3390/ma15010242.
[52] *SCIA Engineer*. (2026). Nemetschek Group. Accessed: Jan. 27, 2026. [Online]. Available: https://www.scia.net/fr/scia-engineer
[53] European Committee for Standardization, *EN 338:2016: Structural Timber - Strength classes*, Jun. 30, 2016.
[54] B. Heimeshoff, 'Zur Berechnung von Biegeträgern aus nachgiebig miteinander verbundenen Querschnittsteilen im Ingenieurholzbau', *Holz als Roh-und Werkstoff*, vol. 45, no. 6, pp. 237–241, Jun. 1987, doi: 10.1007/BF02616416.
[55] European Committee for Standardization, 'B5. Mechanically jointed members', in *EN 1995-1-1:2025 Eurocode 5: Design of timber structures - Part 1-1: General rules and rules for buildings*, Brussels (Belgium), 2025.
[56] H. J. Blaß and C. Sandhaas, 'D7. Mechanically jointed members and CLT elements', in *Timber Engineering: Principles for Design*, Karlsruhe: KIT Scientific Publishing, 2017.
[57] M. Wallner-Novak, J. Koppelhuber, and K. Pock, *Cross-Laminated Timber Structural Design - Basic design and engineering principles according to Eurocode*. Wien: ProHolz Austria, 2014.
[58] H. Kreuzinger, 'Platten, Scheiben und Schalen', in *Bauen mit Holz*, vol. 101, 1999.

[59] U. A. Girhammar and V. K. A. Gopu, ‘Composite Beam-Columns with Interlayer Slip—Exact Analysis’, *J. Struct. Eng.*, vol. 119, no. 4, pp. 1265–1282, Apr. 1993, doi: 10.1061/(ASCE)0733-9445(1993)119:4(1265).
[60] U. A. Girhammar and D. H. Pan, ‘Exact static analysis of partially composite beams and beam-columns’, *International Journal of Mechanical Sciences*, vol. 49, no. 2, pp. 239–255, Feb. 2007, doi: 10.1016/j.ijmecsci.2006.07.005.
[61] European Committee for Standardization, *EN 408+A1:2012: Timber structures - Structural timber and glued laminated timber - Determination of some physical and mechanical properties*, Brussels (Belgium)., Sep. 28, 2012.
[62] European Committee for Standardization, *EN 12512:2002: Timber structures - Test methods - Cyclic testing of joints made with mechanical fasteners*, Jan. 09, 2002.
[63] Yusof Ahmad, ‘Ductility of Timber Beams Strengthened Using Fiber Reinforced Polymer’, *JCEA*, vol. 7, no. 5, May 2013, doi: 10.17265/1934-7359/2013.05.003.
[64] F. J. Rescalvo, C. Timbolmas, R. Bravo, I. Valverde-Palacios, and A. Gallego, ‘Improving ductility and bending features of poplar glued laminated beams by means of embedded carbon material’, *Construction and Building Materials*, vol. 304, p. 124469, Oct. 2021, doi: 10.1016/j.conbuildmat.2021.124469.
[65] H. Fu, Z. Li, and M. He, ‘Experimental research on flexural performance of dowel laminated timber composed of LVL made from fast-growing larch’, *Eur. J. Wood Prod.*, vol. 83, no. 2, p. 81, Mar. 2025, doi: 10.1007/s00107-025-02239-7.
[66] A. Sotayo, D. Bradley, M. Bather, M. Oudjene, I. el Houjeyri, and Z. Guan, ‘Development and structural behaviour of adhesive free laminated timber beams and cross laminated panels’, *Construction and Building Materials*, vol. 259, p. 119821, Oct. 2020, doi: 10.1016/j.conbuildmat.2020.119821.
[67] Y.-H. Yeh, Y.-C. Yeh, Y.-H. Yeh, and Y.-C. Yeh, ‘Bending Behaviour and Failure Modes of Non-Glue-Laminated Timber Beams Composed of Wooden Dowels and Self-Tapping Screws’, *Buildings*, vol. 14, no. 2, Feb. 2024, doi: 10.3390/buildings14020394.